Hydrothermal synthesis of α-MnO$_2$ nanorods and its electrochemical characterization for supercapacitor applications

Syam G. Krishnan, Midhun Harilal, Mohd. Hasbi Ab Rahim and Rajan Jose[*]
Nanostructured Renewable Energy Materials Laboratory,
Faculty of Industrial Sciences and Technology, Universiti Malaysia Pahang,
26300 Kuantan, Malaysia
Corresponding author :- rjose@ump.edu.my

Abstract— MnO$_2$ is considered as a candid material for supercapacitor applications owing to its varied oxidation states, environmental friendliness and low cost. α-MnO$_2$ nanorods is synthesized by a facile hydrothermal method and is characterized by X-ray Diffraction, Field Emission Scanning Electron Microscopy, gas adsorption studies, cyclic voltammetry, Galvanostatic charge-discharge studies and Electrochemical impedance spectroscopy. The α-MnO$_2$ demonstrated a promising specific capacitance of ~310 F g^{-1} at a current density of 1 A g^{-1} with lower contact resistance in 3M LiOH.

Keywords— Supercapacitor, α-MnO$_2$, Energy storage devices, Transition metal oxides.

1. INTRODUCTION

Smarter and efficient energy storage devices are under huge demand owing to the increasing popularity of hybrid vehicles and wireless devices. Such need for the wireless devices are now accomplished by batteries especially, lithium ion or lithium polymer batteries, which are characterized by lower power density (~300 W Kg^{-1}) and larger energy density (~150 Wh Kg^{-1}). For hybrid vehicles, the major challenge in using these rechargeable batteries (usually nickel metal hydrate battery) are its lower cycle life (500 cycles) and power variation at different climatic conditions. To address those concerned issues, supercapacitor, an advanced energy storage device with higher power density can be used along with the higher energy density rechargeable batteries. Electric double layer capacitance (EDLC) employing non faradic charge transfer process, pseudocapacitors using faradic charge transfer process and hybrid capacitors merging the two storage modes are the three categories of supercapacitor. The pseudocapacitive properties of RuO$_2$[1], MnO$_2$[2], Co$_3$O$_4$[3], CuO[4] and NiO[5] were studied while carbons (carbon nanotubes[6] , graphene[7] and activated carbon[8]) were explored for its EDLC properties. Recently the electrochemical properties of electrospun CuO[9], Co$_3$O$_4$[10] and NiO[11] nanowires as well as hydrothermal synthesized MnO$_2$ nanoflowers[12] were explored by our group for pseudocapacitor applications. The specific capacitance (C$_S$) of these materials ranged from ~300 F g^{-1} to ~1100 F g^{-1} at a current density of 1 A g^{-1} with coulombic efficiency (η) ranging from ~92 to ~99% and capacitance retention from 95 to 100% after 1000 to 3000 cycles. Our group also explored the performance of ternary cobaltites[13,14] for pseudocapacitor application and obtained promising results.

The electrochemical characterization of various forms of MnO$_2$ (α, γ, and δ)[9] were explored for supercapacitor application. Neutral electrolytes such as Na$_2$SO$_4$, K$_2$SO$_4$ are used for its electrochemical characterization. However, fewer attempts are made for its electrochemical studies in alkaline electrolytes. The electrochemical characterization of α-MnO$_2$ nanorods in 3M LiOH are reported for the first time and the study promises greater significance of exploring α-MnO$_2$ nanorods as a high performance supercapacitor electrode.

2. EXPERIMENTAL DETAILS

2.1. Synthesis and Characterization of α-MnO$_2$

α-MnO$_2$ powders were synthesized using a simple hydrothermal technique. 2 mmol KMnO$_4$ and 300μL of 30 Wt% HCl were dissolved in 40 mL deionized water and magnetically stirred for 15 minutes. The dark red solution is transferred to a teflon lined stainless steel autoclave and placed in a pre-heated oven at 140 ^{o}C for 12 hours and cooled to room temperature. The resultant brown products are filtered and washed many times with water and ethanol. The washed product is vacuum dried at 60 ^{o}C in an oven.

XRD (Rigaku miniflex II) consisting CuKα radiation (λ = 1.5406 Å) was employed in exploring the crystal structure while surface properties of powders are explored using a Tristar 3000 (Micrometrics, USA) instrument. Field emission scanning electron microscopy (FESEM; 7800F, JEOL, USA) was used to detect the morphology of the MnO_2 powders.

2.2. Electrode preparation and eletrochemical studies

The working electrode was prepared by mixing 75% of $MgCo_2O_4$ powder with polyvinylidenefluoride (PVDF) (Sigma Aldrich, USA) and carbon black (conductive Super P, Alfa Aesar, UK) in the ratio 75: 15: 10. The homogeneity of the solution was ensured with the use of N- methyl-2-pyrrolidone (NMP) as a solvent. This homogeneous paste was then coated on to area of $1cm^2$ of a pre-cleaned nickel substrates and dried in an oven at 60 ^oC for 24 hours. The dried electrodes are further pressed at a pressure of 5 ton using a hydraulic press. Cyclic Voltammetry (CV), galvanostatic charge – discharge cycling (CD) and electrochemical impedance spectroscopy (EIS) measurements are performed to study electrochemical properties of the electrode. A three electrode configuration (working electrode, Platinum rod and saturated Ag/ AgCl) is used for electrochemical studies at room temperature using a galvanostatic potentiostat (PGSTAT M101, Metrolab Autloab B.V, The Netherlands) consisting Nova 1.9 software.
.

3. RESULTS AND DISCUSSION

3.1. Crystal structure and morphology of MnO_2 powder

Fig. 1(a) shows the XRD pattern of the material which reveals its polycrystallinity and phase information. Sharp peaks were obtained for (211) plane followed by (411) and (521) planes. All the peaks fit well to the reported tetragonal phase (JCPDS 44-0141) having space group I4/m with lattice parameters a = 9.74 Å and c = 2.85 Å.

The gas adsorption studies revealed the BET surface area of the powder to be 45.3 $m^2 g^{-1}$ and the average pore width determined using Barett – Joyner – Halenda (BJH) analysis to be 90 Å. The contribution from compact ion layer in the neighboring ion wall may increase the supercapacitive property owing to the higher pore width of the MnO_2 powder than the solvated ion size[15].

Fig. 1(b) shows the FESEM of the powders which revealed in its nanorod morphology. This nanorods with acceptable surface area and larger pore size can improve the charge polarization thereby improving the pseudocapacitance.
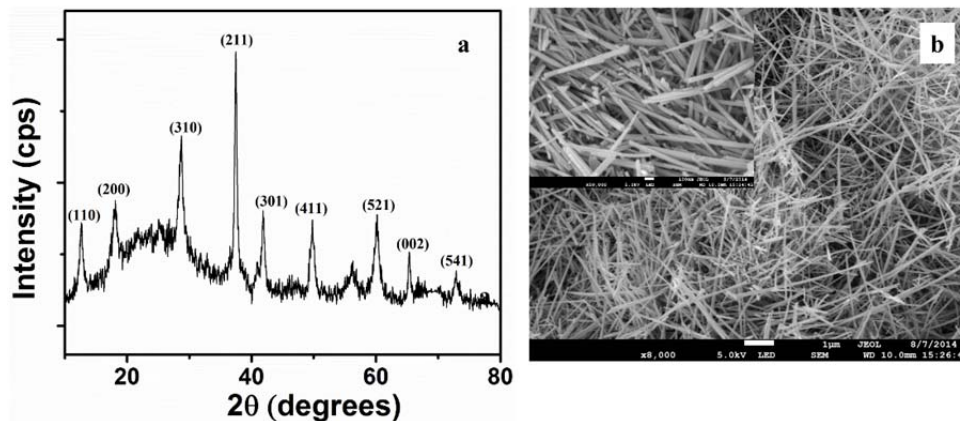

Figure:1 (a) XRD of α-MnO_2 nanorods (b) FESEM of α-MnO_2 nanorods; inset with a higher magnification of 100 nm.

3.2 Electrochemical characterization of α-MnO_2 electrodes

CV studies were performed in a three electrode configuration so as to explore the supercapacitive behavior of the electrode material in 3M LiOH. Fig. 2 (a) shows CV curves at varying current density. All the scan rate depicts well defined reduction and oxidation peaks which can be attributed to the faradic reaction of Mn^{4+}/Mn^{3+} with H^+ ions thereby proving its usefulness as a pseudocapacitor electrode. Redox peaks for the CV measurements can be explained using the Equation (1)[16]

$$MnO_2 + H^+ + e^- \underset{Discharging}{\overset{charging}{\rightleftarrows}} MnOOH \qquad (1)$$
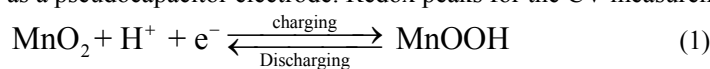
The ratio of anodic and cathodic area (Coulombic efficiency, η) remained at ~96% indicating good electrochemical reversibility. This higher η shall improve the capacity retention of the electrode to obtain longer cycle life. The shift in the redox peaks while shifting from higher to lower scan rates in Fig. 2(a) clearly demonstrates the electrical polarization in the electrode.

Fig- 2(b) demonstrates specific capacitance (C_S) variation with scan rate. The C_S of the electrode can be calculated using

$$C_S = \frac{1}{mv[E_2 - E_1]} \int_{E_1}^{E_2} i(E)dE \qquad (2)$$

where 'm' is the mass of the active material, 'v' is the scan rate, '$E_2 - E_1$' provide the potential window and '$i(E)$' is the current at respective potential.

The C_S of the electrode at a scan rate of 2 mV s^{-1} were calculated to be ~325 F g^{-1}. As the scan rate increased, the C_S decreased owing to (i) the variation of active sites accessed by H$^+$ ions and (ii) the dominance of EDLC over PC at higher scan rates due to the restricted ion movement at higher scan rates[14].

The inset of Fig.2(b) demonstrates a straight line fit indicating that the capacitance is originated from a semi-infinite bulk intercalation ($i \propto \sqrt{v}$) than surface redox reaction ($i \propto v$)[17]. In short, bulk diffusion of H$^+$ ions dominates its capacitance.
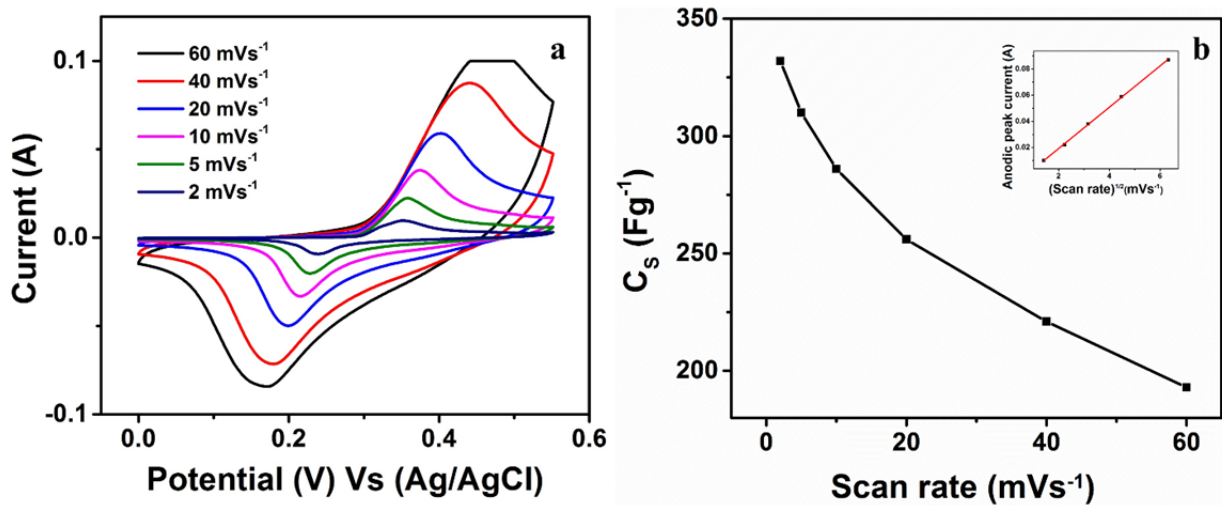

Figure 2 : (a) CV curve of α-MnO$_2$ electrode at various scan rate (b) Variation of C$_s$ with various scan rate; inset, variation of anodic peak current with square root of scan rate.

Fig.3 show the Galvanostatic CD curves at a current density of 1 Ag^{-1} which aids in further evaluating the supercapacitive performance of electrodes. The CD curves demonstrates an asymmetric shape indicating the faradic behavior of the material. The lower (~8 mV) initial potential drop (V_{IR}) indicates improved faradic reaction as well as its lower internal resistance (1.2 Ω); which can be obtained from the ratio of V_{IR} and corresponding discharge current (I_D), might have contributed to its improved capacitance. The inset of the Fig.3(b) shows the variation of C_S at different current densities. The C_s decreased as current density increased similar to the measurements obtained from CV.

The C$_S$ of the electrode from CD measurements can be obtained from the equation

$$C_s = \frac{It}{m\Delta V} \qquad (3)$$

where I, t, m and ΔV are applied current, discharge time, active mass and potential difference, respectively. The C_S of the active material was ~325 F g^{-1} at a current density of 1 A g^{-1}. The larger pore size of the active material compared to H$^+$ ions and improved BET surface area as well as nanoflower structure might have resulted in its improved capacitance.

The discharge CD curves for various current densities is shown in Fig 3 (b). The C_S decreased to 49% of its initial value when the current density is increased by 10 times. This decrease might have occurred owing to the lesser utilization of active material at higher current densities thereby decreasing the contribution of pseudocapacitance to the total C_s. As it can be observed from Fig 3(b), the faradic reaction occurs in the voltage range between 0.5 to 0.23 V and its range decreases at a high current densities indicating the dominance of EDLC to pseudocapacitance.
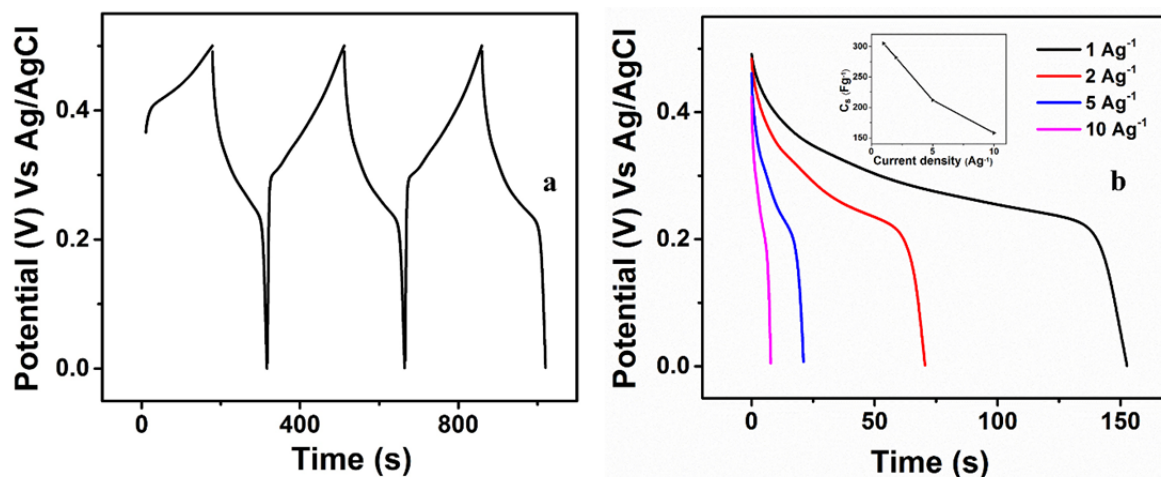
Figure 3: (a) CD curves of α-MnO$_2$ electrodes at 1 Ag^{-1} (b) Discharge curves of α-Mno$_2$ electrodes at various current densities; inset, the variation of C$_S$ with current densities

The cyclic stability of the electrode is important for its practical applicability and stability test under extreme load for 1000 cycles was performed and is shown in Fig.4. The current density for the test was fixed at 5 Ag^{-1}. The capacitance remained constant at ~210 Fg^{-1} for the first 400 cycles. The capacitance started decreasing and at the end of 1000 cycle the capacitance measured was ~180 Fg^{-1} retaining 85% of its initial capacitance. The present nanorod structure tested in 3M LiOH shown an improved capacitance retention than its other counter parts reported earlier.
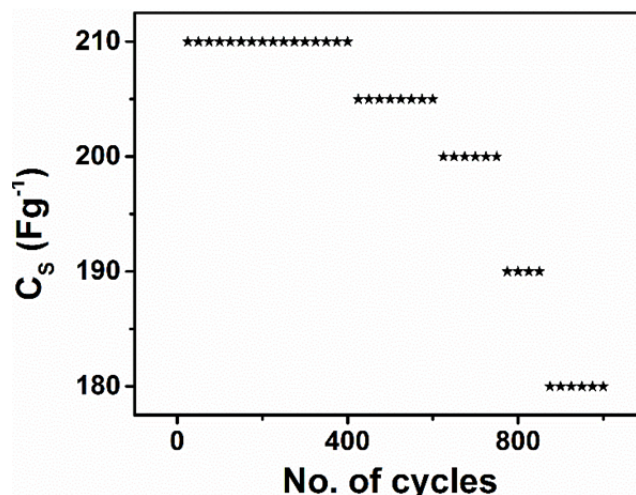

Figure: 4 Cyclic stability of α-MnO$_2$ electrode for 1000 cycles.

The ion transport kinetics of the electrode can be further analyzed from the EIS spectra at open circuit potential. Moreover, the capacitive measurements obtained from CV and CDC experiments can be revalidated by obtaining the characteristic resistances such as electrochemical resistance (R_s) and charge transfer resistance (R_{ct}) from Nyquist plot (Fig.5) of EIS analysis[18]. The R_s value, a combination of (i) electrolyte resistance (ii) intrinsic resistance of electrode and (iii) the contact resistance of between the electrode and the current collector was found to be 0.93 Ω. The lower R_S value may increase its pseudocapacitance as well as its power capability as power density (P) of the pseudocapacitor is equal to $V^2/4R_sm$; where V is the charging potential and 'm' is the active mass of the electrode. 'R_{ct}' of the electrode; which determines the kinetic resistance to the ion transfer, obtained from the diameter of the first semicircle is 0.4 Ω is slightly on the higher side. This higher R_{ct} of the electrode may prevented the smooth flow of ions through the pores of the electrode material leading to the less utilization of active materials resulting in a lower capacitance [19].
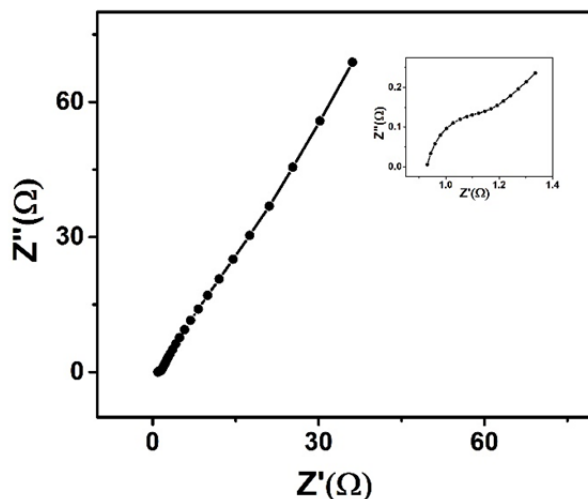
Figure 5: Nyquist plot for α-MnO$_2$ electrode; inset showing high frequency region

4. CONCLUSION

α-MnO$_2$ nanorods were synthesized by a facile hydrothermal method and is studied as electrode for supercapacitor application. The performance of the material as the electrode is supported by CV, CD and EIS studies. The studies were performed in 3M LiOH and the capacitance retention of the material improved than the reported values. The lower value of R_s and R_{ct} promises its application in high performance supercapacitors. Further optimization in the synthesis process may improve the pore size and surface area of the material which can further enhance its C_S.

REFERENCES

[1] C.-C. Hu, K.-H. Chang, M.-C. Lin, Y.-T. Wu, "Design and tailoring of the nanotubular arrayed architecture of hydrous RuO$_2$ for next generation supercapacitors", Nano Lett., 6 (2006) 2690-2695.
[2] S. Kong, K. Cheng, Y. Gao, T. Ouyang, K. Ye, G. Wang, D. Cao, "A novel three-dimensional manganese dioxide electrode for high performance supercapacitors", J. Power Sources, 308 (2016) 141-148.
[3] M. Kumar, A. Subramania, K. Balakrishnan, "Preparation of electrospun Co$_3$O$_4$ nanofibers as electrode material for high performance asymmetric supercapacitors", Electrochim. Acta, 149 (2014) 152-158.
[4] K. Krishnamoorthy, S.-J. Kim, Growth, "Characterization and electrochemical properties of hierarchical CuO nanostructures for supercapacitor applications", Mater. Res. Bull., 48 (2013) 3136-3139.
[5] Y. Zhang, J. Wang, H. Wei, J. Hao, J. Mu, P. Cao, J. Wang, S. Zhao, "Hydrothermal synthesis of hierarchical mesoporous NiO nanourchins and their supercapacitor application", Mater. Lett., 162 (2016) 67-70.
[6] D.N. Futaba, K. Hata, T. Yamada, T. Hiraoka, Y. Hayamizu, Y. Kakudate, O. Tanaike, H. Hatori, M. Yumura, S. Iijima, "Shape-engineerable and highly densely packed single-walled carbon nanotubes and their application as super-capacitor electrodes", Nat Mater, 5 (2006) 987-994.
[7] E.Y.L. Teo, H.N. Lim, R. Jose, K.F. Chong, "Aminopyrene functionalized reduced graphene oxide as a supercapacitor electrode", RSC Adv., 5 (2015) 38111-38116.
[8] F. Barzegar, A. Bello, D. Momodu, M.J. Madito, J. Dangbegnon, N. Manyala, "Preparation and characterization of porous carbon from expanded graphite for high energy density supercapacitor in aqueous electrolyte", J. Power Sources, 309 (2016) 245-253.
[9] B. Vidhyadharan, I.I. Misnon, R.A. Aziz, K.P. Padmasree, M.M. Yusoff, R. Jose, "Superior supercapacitive performance in electrospun copper oxide nanowire electrodes", J. Mater. Chem. A, 2 (2014) 6578-6588.
[10] B. Vidhyadharan, R.A. Aziz, I.I. Misnon, G.M. Anil Kumar, J. Ismail, M.M. Yusoff, R. Jose, "High energy and power density asymmetric supercapacitors using electrospun cobalt oxide nanowire anode", J. Power Sources, 270 (2014) 526-535.
[11] B. Vidhyadharan, N.K.M. Zain, I.I. Misnon, R.A. Aziz, J. Ismail, M.M. Yusoff, R. Jose, "High performance supercapacitor electrodes from electrospun nickel oxide nanowires", J. Alloy. Compd., 610 (2014) 143-150.
[12] I.I. Misnon, R.A. Aziz, N.K.M. Zain, B. Vidhyadharan, S.G. Krishnan, R. Jose, "High performance MnO$_2$ nanoflower electrode and the relationship between solvated ion size and specific capacitance in highly conductive electrolytes", Mater. Res. Bull., 57 (2014) 221-230.
[13] S.G. Krishnan, M.H.A. Rahim, R. Jose, "Synthesis and characterization of MnCo$_2$O$_4$ cuboidal microcrystals as a high performance psuedocapacitor electrode", J. Alloy Compd., 656 (2016) 707-713.

[14] S.G. Krishnan, M.V. Reddy, M. Harilal, B. Vidyadharan, I.I. Misnon, M.H.A. Rahim, J. Ismail, R. Jose, "Characterization of $MgCo_2O_4$ as an electrode for high performance supercapacitors", Electrochim. Acta, 161 (2015) 312-321.

[15] C. Largeot, C. Portet, J. Chmiola, P.-L. Taberna, Y. Gogotsi, P. Simon, "Relation between the ion size and pore size for an electric double-layer capacitor", J. Am. Chem. Soc., 130 (2008) 2730-2731.

[16] S.C. Pang, M.A. Anderson, T.W. Chapman, "Novel electrode materials for thin-film ultracapacitors: comparison of electrochemical properties of sol-gel-derived and electrodeposited manganese dioxide", J. Electrochem. Soc., 147 (2000) 444-450.

[17] J. Chmiola, G. Yushin, Y. Gogotsi, C. Portet, P. Simon, P.L. Taberna, "Anomalous increase in carbon capacitance at pore sizes less than 1 nanometer", Science, 313 (2006) 1760-1763.

[18] S.K. Meher, G.R. Rao, "Ultralayered Co_3O_4 for high-performance supercapacitor applications", J. Phys. Chem. C, 115 (2011) 15646-15654.

[19] F. Lisdat, D. Schäfer, "The use of electrochemical impedance spectroscopy for biosensing", Anal. Bioanal. Chem., 391 (2008) 1555-1567.